Proceedings of the Eighteenth International Conference on
Civil, Structural and Environmental Engineering Computing
Edited by: P. Iványi, J. Kruis and B.H.V. Topping
Civil-Comp Conferences, Volume 10, Paper 8.2
Civil-Comp Press, Edinburgh, United Kingdom, 2025
ISSN: 2753-3239, doi: 10.4203/ccc.10.8.2

Fictitious Domain Approach for a Fluid in an Elastic Channel

L. Gastaldi and P. Tesini

Dipartimento di Ingegneria Civile, Architettura, Territorio, Ambiente e di Matematica (DICATAM), Università degli Studi di Brescia, Italy

Abstract

We consider a fluid structure interaction problem consisting of a channel with an elastic wall which deforms due to the flow of an incompressible fluid. The proposed method consists in the use of a fictitious domain approach so that the fluid domain is extended outside the channel and the structure is then immersed in the fluid. This allows to avoid the construction of a time dependent grid fitted with the position of the structure. Our results are in good agreement with those provided by a remeshing technique.

Keywords: fluid structure interactions, fictitious domain method, immersed boundary method, finite elements, incompressible fluid, elastic response.

1 Introduction

Fluid-structure interaction is a fundamental research field in engineering and applied sciences, as it analyzes the dynamic interactions between fluids and solid structures

(see, e.g., [1–4]) and a thorough understanding of these phenomena is essential in numerous applications, ranging from the stability of aerodynamic structures to cardiovascular biomechanics.

The immersed boundary method, represents an early and influential approach for simulating fluid-structure interactions. This method has been successfully applied to simulate blood flow around simplified heart valve geometries, demonstrating the method's ability to handle fluid-structure interactions in biomedical scenarios [5]. In [6,7], the authors developed and analyzed a formulation based on the fictitious domain method [8,9] that uses a Lagrange multiplier within the immersed boundary method.

In this framework, the fictitious domain method emerges as an effective approach for simulating fluid-structure interaction problems, especially in scenarios involving big deformations of solid structures. This method extends the fluid domain to include the regions occupied by solid structures, facilitating the modeling of interactions without the need for continuous remeshing during simulations. This approach allows to use grids in the solid and in the fluid domains totally independent from each other, reducing the errors associated with remeshing. The price to pay are coupling terms which involve functions defined on the two meshes.

Our present work focuses on the application of the fictitious domain method to model fluid-structure interaction in an elastic channel. Specifically, we want to evaluate the performance of this method in simulating the behavior of a fluid interacting with a deformable channel wall, considered as a thin elastic structure of codimension 1. Through a series of numerical simulations, we analyze the effectiveness of the method in capturing key physical phenomena such as wall deformation, and flow characteristics. The aim is to contribute to the development of a computational tool for simulating fluid-structure interaction systems, particularly in biomedical and engineering applications.

2 Problem setting

We consider, for the fluid motion, a two-dimensional domain $\Omega^{\mathrm{f}}(t)$, evolving in time t, with $t \in [0, T]$. The domain $\Omega^{\mathrm{f}}(t)$ is bounded by different types of boundaries, each playing a specific role in the fluid dynamics.

The fluid inlet boundary is denoted with $\Gamma^{\mathrm{f}}_{\mathrm{in}}$ while $\Gamma^{\mathrm{f}}_{\mathrm{out}}$ represents the outlet boundary. Additionally, the lower boundary $\Gamma^{\mathrm{f}}_{\mathrm{wall}}$ is assumed to be a fixed wall in this study. However, this approach can be extended to consider $\Gamma^{\mathrm{f}}_{\mathrm{wall}}$ as an axis of symmetry of a real system.

The upper boundary, denoted as $\Sigma(t)$, represents an elastic wall that confines the fluid domain and evolves over time due to fluid motion, requiring a coupled fluid-structure interaction approach.

To address this problem, we adopt an approach that introduces a fictitious domain $\Omega^{\mathrm{fd}}(t)$, which extends the real domain $\Omega^{\mathrm{f}}(t)$ and serves as a useful computational tool.

This fictitious domain $\Omega^{\text{fd}}(t)$ is assumed to be filled with the same fluid and is bounded at the lower side by $\Sigma(t)$ and at the other sides by $\Gamma^{\text{fd}}_{\text{out}}$ and $\Gamma^{\text{fd}}_{\text{wall}}$.

We want to formulate an appropriate method with well-posed boundary conditions, ensuring that the solution in $\Omega^{\text{fd}}(t)$ remains purely auxiliary from a computational perspective and does not influence the physical results of interest in $\Omega^{\text{f}}(t)$.

Therefore, we consider a fixed bounded rectangular domain $\Omega \subset \mathbb{R}^d$ (with $d = 2$) with a Lipschitz boundary $\Gamma = \partial\Omega$. Inside Ω, a thin elastic structure $\Sigma(t)$ of codimension 1 is immersed, evolving over time t. The presence of this structure creates the partition of Ω into the two subdomains $\Omega^{\text{fd}}(t)$ and $\Omega^{\text{f}}(t)$, s.t. $\Omega = \Omega^{\text{fd}}(t) \cup \Omega^{\text{f}}(t)$, and the interface $\Sigma(t)$ separates these subdomains (see Figure 1). Moreover, the fixed boundary Γ is composed by distinct parts: $\Gamma = \Gamma^{\text{f}}_{\text{in}} \cup \Gamma^{\text{f}}_{\text{wall}} \cup \Gamma^{\text{f}}_{\text{out}} \cup \Gamma^{\text{fd}}_{\text{out}} \cup \Gamma^{\text{fd}}_{\text{wall}}$.

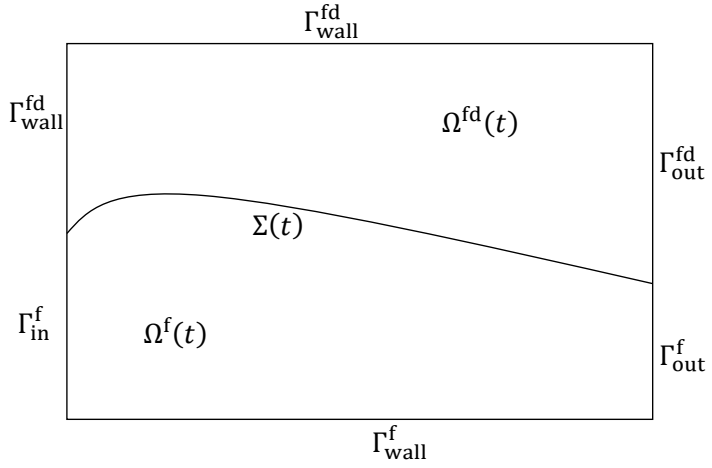

Figure 1: Geometrical setting for the fluid-structure interaction problem.

To describe the motion of the structure, we adopt the Lagrangian framework. Let Σ be a reference domain, corresponding to the rest position of the structure, and $X \in \Sigma$ be the Lagrangian coordinate. We introduce a displacement field $\mathbf{d} : \Sigma \to \mathbb{R}^d$, which defines the deformation mapping $\boldsymbol{\phi} : \Sigma \to \Sigma(t)$ as follows

$$\boldsymbol{\phi}(X, t) = \mathbb{I}(X) + \mathbf{d}(X, t) \quad \text{for } X \in \Sigma, \tag{1}$$

where $\mathbb{I}$ is the identity function on Σ. We assume that this rest position corresponds to the horizontal segment $[0, L]$, and L stands for the length of the rectangular fixed domain Ω.

Denoting with $\mathbf{x} = (x_1, x_2)$ the Eulerian coordinate, the velocity field $\mathbf{u}(\mathbf{x}, t)$ and pressure field $p(\mathbf{x}, t)$ are defined in the entire computational domain Ω and satisfy the fluid equations, treated in Eulerian framework.

In this way, the structure, which is assumed to exhibit elastic behavior, interacts with the fluid through a set of coupling conditions that ensure velocity continuity and force equilibrium, as presented below.

2.1 Governing equations

The evolution of the system, representing the fluid-structure interaction problem, is governed by the equations presented in this section, for both the fluid and solid domains, as well as the coupling conditions at the interface.

2.1.1 Fluid sub-problem

We assume that the fluid dynamic is governed by the incompressible Navier-Stokes equations:

$$\begin{cases} \rho^f(\partial_t \mathbf{u} + \mathbf{u}\cdot\nabla\mathbf{u}) - \nabla\cdot\boldsymbol{\sigma}^f = 0 & \text{in } \Omega, \\ \nabla\cdot\mathbf{u} = 0 & \text{in } \Omega, \end{cases} \tag{2}$$

where ρ^f is the fluid density and $\boldsymbol{\sigma}^f$ denotes the Cauchy stress tensor: $\boldsymbol{\sigma}^f := -p\mathbb{I} + 2\mu\boldsymbol{\epsilon}(\mathbf{u})$. Here μ stands for the dynamic viscosity coefficient, specific of the fluid and $\boldsymbol{\epsilon}$ is the strain tensor $\boldsymbol{\epsilon}(\mathbf{u}) := \frac{1}{2}\left(\nabla\mathbf{u} + \nabla\mathbf{u}^T\right)$.

2.1.2 Solid sub-problem

The elastic structure is governed by the structural dynamics:

$$\begin{cases} \rho^s\,\varepsilon\,\partial_t\dot{\mathbf{d}} + \mathbf{L}\mathbf{d} = \mathbf{f}_\Sigma & \text{on } \Sigma, \\ \partial_t\mathbf{d} = \dot{\mathbf{d}} & \text{on } \Sigma, \end{cases} \tag{3}$$

where ρ^s is the solid density and ε represents the real thickness of the thin structure, treated in the present work as a codimension-1 manifold. Moreover, we assume that the operator $\mathbf{L}\mathbf{d}$ accounts for the internal elastic forces described in the setting of the linear elasticity. In particular, we consider

$$\mathbf{L}\mathbf{d} = -\kappa\,\Delta\mathbf{d},$$

where κ is the constant Lamé coefficient, computable through to the Young's modulus (E) and Poisson's coefficient (ν), specific to the elastic material: $\kappa = \frac{\varepsilon\,E}{2(1+\nu)}$. The quantity $\mathbf{f}_\Sigma$ represents the resultant force term applied on the surface Σ, which includes both the external forces acting on the structure, assumed negligible in our case, and the contribution of the fluid-structure interaction forces arising from the coupling conditions, which is therefore treated as an unknown of the problem.

2.1.3 Interface coupling conditions

To ensure the proper interaction between the fluid and solid domains, we impose the following coupling conditions at the interface:

$$\begin{cases} \boldsymbol{\phi} = \mathbb{I} + \mathbf{d} & \text{on } \Sigma, \\ \mathbf{u}\circ\boldsymbol{\phi} = \dot{\mathbf{d}} & \text{on } \Sigma, \\ \int_\Sigma \mathbf{f}_\Sigma\cdot\mathbf{w} = -\int_{\Sigma(t)}[\![\boldsymbol{\sigma}^f\mathbf{n}^{\Sigma(t)}]\!]\cdot\mathbf{w}\circ\boldsymbol{\phi}^{-1}(\cdot,t) & \forall\mathbf{w}:\Sigma\to\mathbb{R}^d \text{ smooth}, \end{cases} \tag{4}$$

where, $[\![\cdot]\!]$ denotes the jump across the interface, while $\mathbf{n}^{\Sigma(t)}$ is the unit normal vector to the interface $\Sigma(t)$, and $\boldsymbol{\sigma}^f \mathbf{n}^{\Sigma(t)}$ represents the normal stress across the interface.

2.1.4 Boundary conditions

To properly complete our model problem, we impose suitable boundary conditions on the external domain boundary, to ensure that the solution of the problem in the fictitious part of the domain $\Omega^{\text{fd}}(t)$ does not affect the physical part of interest $\Omega^{\text{f}}(t)$.

In particular, at the inlet boundary $\Gamma^{\text{f}}_{\text{in}}$, we impose:

$$\mathbf{u} \cdot \mathbf{n}^{\text{f,in}} = u_{\text{in}}, \qquad \mathbf{n}^{\text{f,in}} \cdot (\boldsymbol{\sigma}^f \mathbf{t}^{\text{f,in}}) = 0 \quad \text{on } \Gamma^{\text{f}}_{\text{in}}, \tag{5}$$

where u_{in} is the inlet profile, $\mathbf{n}^{\text{f,in}}$ the unit normal vector to $\Gamma^{\text{f}}_{\text{in}}$ and $\mathbf{t}^{\text{f,in}}$ the unit tangent vector along $\Gamma^{\text{f}}_{\text{in}}$,

On the boundaries $\Gamma^{\text{f}}_{\text{out}}$ and $\Gamma^{\text{fd}}_{\text{out}}$, the natural choice is the homogeneous Neumann condition and, denoting with $\mathbf{n}^{\text{out}}$ the unit normal vector to $\Gamma^{\text{f}}_{\text{out}} \cup \Gamma^{\text{fd}}_{\text{out}}$, we can write:

$$\boldsymbol{\sigma}^f \mathbf{n}^{\text{out}} = 0 \quad \text{on } \Gamma^{\text{f}}_{\text{out}} \cup \Gamma^{\text{fd}}_{\text{out}}. \tag{6}$$

Moreover, on the wall boundaries $\Gamma^{\text{f}}_{\text{wall}} \cup \Gamma^{\text{fd}}_{\text{wall}}$, we impose homogeneous Dirichlet condition, enforcing a no-slip condition on the velocity field:

$$\mathbf{u} = 0 \quad \text{on } \Gamma^{\text{f}}_{\text{wall}} \cup \Gamma^{\text{fd}}_{\text{wall}}.$$

Regarding $\mathbf{d}$, at $X = 0$ we impose a homogeneous Dirichlet condition on the entire displacement vector, and at $X = L$, we fix the first component to be zero, while the second one satisfy a natural Neumann condition,

$$\mathbf{d} = 0 \quad \text{at } X = 0, \qquad d_1 = 0, \ \frac{\partial d_2}{\partial X} = 0 \quad \text{at } X = L.$$

2.1.5 Initial conditions

The system is completed with the following initial conditions regarding fluid velocities, as well as the structure displacements and structure velocities:

$$\begin{cases} \mathbf{u}(\cdot, 0) = \mathbf{u}_0 & \text{in } \Omega, \\ \mathbf{d}(\cdot, 0) = 0, \quad \dot{\mathbf{d}}(\cdot, 0) = \mathbf{u}_0 & \text{on } \Sigma. \end{cases}$$

where $\mathbf{u}_0$, is the given initial conditions for the fluid velocity. We assume that the structure is initially at rest, while its time derivative should be equal to the fluid initial velocity, as prescribed in (4).

2.2 Functional spaces and weak formulation

In view of the finite element discretization, we write the problem in weak form. We set:

$$\begin{aligned}
&\mathbf{V} = \left\{\mathbf{v} \in H^1(\Omega) \,:\, \mathbf{v} = 0 \ \text{ on } \Gamma^{\text{f}}_{\text{wall}} \cup \Gamma^{\text{fd}}_{\text{wall}}\right\},\\
&\mathbf{V}_0 = \left\{\mathbf{v} \in \mathbf{V} \,:\, \mathbf{v}\cdot\mathbf{n}^{\text{f,in}} = 0 \ \text{ on } \Gamma^{\text{f}}_{\text{in}}\right\},\\
&\mathbf{W} = \left\{\mathbf{w} \in H^1(\Sigma) \,:\, \mathbf{w}(0) = 0 \ \text{ and } \ w_1(L) = 0\right\},\\
&\boldsymbol{\Lambda} = H^{-1/2}(\Sigma)^d.
\end{aligned}$$

Moreover, for $\boldsymbol{\mu} \in \boldsymbol{\Lambda}$ and $\mathbf{y} \in H^{1/2}(\Sigma)^d$, we set

$$c(\boldsymbol{\mu}, \mathbf{y}) := \langle \boldsymbol{\mu}, \mathbf{y} \rangle,$$

where $\langle \cdot, \cdot \rangle$ stands for the duality pairing between $\boldsymbol{\Lambda}$ and $H^{1/2}(\Sigma)^d$. Thus, we can enforce the continuity of velocity between the fluid and the structure (see (4)) in weak form as:

$$c(\boldsymbol{\mu}, \mathbf{u}\circ\boldsymbol{\phi} - \dot{\mathbf{d}}) = 0 \quad \forall \boldsymbol{\mu} \in \boldsymbol{\Lambda}.$$

Starting from the governing equations presented in Section 2.1, we multiply by suitable functions $\mathbf{v}$, q, and $\mathbf{w}$ and exploit integration by parts. Hence, for the fluid, taking into account the boundary conditions on Γ, we have for all $\mathbf{v} \in \mathbf{V}_0$ and $q \in L^2(\Omega$,

$$\rho^f(\partial_t \mathbf{u}, \mathbf{v}) + b(\mathbf{u}, \mathbf{u}, \mathbf{v}) + a^f(\mathbf{u}, p; \mathbf{v}, q) - \left\langle [\![\sigma^f \mathbf{n}^{\Sigma(t)}]\!], \mathbf{v} \right\rangle = 0, \tag{7}$$

where $(\cdot, \cdot)$ denotes the L^2 inner product on the appropriate domain, and

$$\begin{aligned}
&b(\mathbf{u}, \mathbf{v}, \mathbf{w}) := \frac{\rho^f}{2}\left((\mathbf{u}\cdot\nabla\mathbf{v}, \mathbf{w}) - (\mathbf{u}\cdot\nabla\mathbf{w}, \mathbf{v})\right),\\
&a^f(\mathbf{u}, p; \mathbf{v}, q) := 2\mu\left(\boldsymbol{\epsilon}(\mathbf{u}), \boldsymbol{\epsilon}(\mathbf{v})\right) - (p, \nabla\cdot\mathbf{v}) - (q, \nabla\cdot\mathbf{u}).
\end{aligned}$$

The dynamics of the thin elastic structure can be rewritten, for all $\mathbf{w} \in \mathbf{W}$, as

$$\rho^s \varepsilon(\partial_t \dot{\mathbf{d}}, \mathbf{w})_\Sigma + a^s(\mathbf{d}, \mathbf{w}) = {}_{(H^1(\Sigma))'}\left\langle \mathbf{f}_\Sigma, \mathbf{w} \right\rangle_{H^1(\Sigma)}, \tag{8}$$

where $a^s(\mathbf{d}, \mathbf{w}) := \kappa(\nabla\mathbf{d}, \nabla\mathbf{w})_\Sigma$.

Finally, to ensure the proper coupling of the interaction forces between the fluid and the structure, we introduce the Lagrange multiplier $\boldsymbol{\lambda} \in \boldsymbol{\Lambda}$ and set $\boldsymbol{\lambda} = \mathbf{f}_\Sigma$.

2.3 Weak formulation of the problem

The weak formulation of our model problem reads: given $\mathbf{u}_0$, $\forall t \in (0,T)$, find $\mathbf{u}(t) \in \mathbf{V}$, with $\mathbf{u}(t) \cdot \mathbf{n}^{\text{f,in}} = u_{\text{in}}$ on $\Gamma^{\text{f}}_{\text{in}}$, $p(t) \in L^2(\Omega)$, $\mathbf{d}(t) \in \mathbf{W}$ and $\boldsymbol{\lambda}(t) \in \boldsymbol{\Lambda}$, such that

$$\begin{cases} \rho^f(\partial_t \mathbf{u}(t), \mathbf{v}) + b(\mathbf{u}(t), \mathbf{u}(t), \mathbf{v}) + a^f((\mathbf{u}(t), p(t)), (\mathbf{v}, q)) \\ \qquad\qquad + c(\boldsymbol{\lambda}(t), \mathbf{v} \circ \boldsymbol{\phi}(t)) = 0 \quad \forall (\mathbf{v}, q) \in \mathbf{V}_0 \times L^2(\Omega), \\ \rho^s \varepsilon(\partial_t \dot{\mathbf{d}}(t), \mathbf{w})_\Sigma + a^s(\mathbf{d}(t), \mathbf{w}) - c(\boldsymbol{\lambda}(t), \mathbf{w}) = 0 \quad \forall \mathbf{w} \in \mathbf{W}, \\ c(\boldsymbol{\mu}, (\mathbf{u} \circ \boldsymbol{\phi})(t) - \dot{\mathbf{d}}(t)) = 0 \quad \forall\, \boldsymbol{\mu} \in \boldsymbol{\Lambda}, \\ \dot{\mathbf{d}}(t) = \partial_t \mathbf{d}(t), \\ \boldsymbol{\phi}(t) = \mathbb{I} + \mathbf{d}(t) \quad \text{on } \Sigma. \end{cases} \tag{9}$$

This system encapsulates the interaction between the fluid domain Ω and the immersed elastic structure $\Sigma(t)$, ensuring both dynamic coupling and mechanical equilibrium.

3 Numerical method

For the numerical discretization of the first equation in (9), we construct a fixed background mesh, which does not need to conform to the moving interface $\Sigma(t)$. Let $\mathcal{T}_h$ be a shape regular triangulation of Ω, with mesh size h. Additionally, a separate 1D mesh is defined on the reference domain Σ by subdividing it in a finite number of intervals.

The discrete velocity field $\mathbf{u}_h$ belongs to the finite element space $\mathbf{V}_h \subset \mathbf{V}$, containing continuous piecewise quadratic functions enriched with bubble functions. The pressure p is discretized in $Q_h \subset L^2(\Omega)$, using piecewise linear discontinuous elements. The pair $(\mathbf{V}_h, Q_h)$ satisfies the *inf-sup* stability condition [10], ensuring a stable mixed formulation. The displacement of the structure $\mathbf{d}$ is approximated in the space $\mathbf{W}_h \subset \mathbf{W}$, using $\mathbb{P}_2$ elements.

Finally, the discrete Lagrange multiplier $\boldsymbol{\lambda}_h$, associated to the kinematic coupling condition, belongs to the space $\boldsymbol{\Lambda}_h \subset \boldsymbol{\Lambda}$ and is composed by continuous piecewise quadratic elements.

We choose quadratic elements for the fluid velocity and for the displacement to capture fine-scale fluid and structure dynamics, while the discontinuous piecewise linear pressure elements provide flexibility in handling interactions and potential jumps at the fluid-structure interface.

For time discretization, we use a modified backward Euler scheme, which incorporates the interface position and the velocity at the previous time step in the coupling and in the convection term, respectively. Given a uniform time step $\Delta t = T/M$, where M is a positive integer, we denote the discrete time levels as $t^n = n\Delta t$ and we can adopt the approximations: $\partial_t \mathbf{u}_h^n \approx \frac{\mathbf{u}_h^n - \mathbf{u}_h^{n-1}}{\Delta t}$, and $\partial_t \mathbf{d}_h^n \approx \frac{\mathbf{d}_h^n - \mathbf{d}_h^{n-1}}{\Delta t}$.

In this way, we can write the discrete formulation of Problem (9) presented in Section 2.3: given $\mathbf{u}_0$, for $n = 1, \ldots, M$, find $\mathbf{u}_h^n \in \mathbf{V}_h$, with $\mathbf{u}_h^n \cdot \mathbf{n}^{\text{f,in}}(t^n) = u_{\text{in}}$ on

$\Gamma^{\mathrm{f}}_{\mathrm{in}}$, $p_h^n \in Q_h$, $\mathbf{d}^n \in \mathbf{W}_h$ and $\boldsymbol{\lambda}_h^n \in \boldsymbol{\Lambda}_h$, such that

$$
\begin{cases}
\rho^f \left(\dfrac{\mathbf{u}_h^n - \mathbf{u}_h^{n-1}}{\Delta t}, \mathbf{v}_h \right) + b(\mathbf{u}_h^{n-1}, \mathbf{u}_h^n, \mathbf{v}_h) + a^f((\mathbf{u}_h^n, p_h^n), (\mathbf{v}_h, q_h)) \\
\qquad\qquad c(\boldsymbol{\lambda}_h^n, \mathbf{v}_h \circ \boldsymbol{\phi}_h^{n-1}) = 0 \qquad\qquad \forall (\mathbf{v}_h, q_h) \in \mathbf{V}_h \times Q_h, \\
\rho^s \varepsilon \left(\dfrac{\dot{\mathbf{d}}_h^n - \dot{\mathbf{d}}_h^{n-1}}{\Delta t}, \mathbf{w}_h \right)_\Sigma + a^s(\mathbf{d}_h^n, \mathbf{w}_h) - c(\boldsymbol{\lambda}_h^n, \mathbf{w}_h) = 0 \quad \forall \mathbf{w}_h \in \mathbf{W}_h, \\
c(\boldsymbol{\mu}_h^n, \mathbf{u}_h^n \circ \boldsymbol{\phi}_h^{n-1} - \dot{\mathbf{d}}_h^n) = 0 \qquad\qquad \forall \boldsymbol{\mu}_h \in \boldsymbol{\Lambda}_h, \\
\dot{\mathbf{d}}_h^n = \dfrac{\mathbf{d}_h^n - \mathbf{d}_h^{n-1}}{\Delta t}, \\
\boldsymbol{\phi}_h^n = \mathbb{I} + \mathbf{d}_h^n.
\end{cases}
\tag{10}
$$

3.1 System matrix

At each time step, System (10) corresponds to the following linear system:

$$
\left(\begin{array}{cc|c|c}
\mathbf{A}(\mathbf{u}_h^{n-1}) & \mathbf{B}^\top & \mathbf{0} & \mathbf{L}_f^\top\left(\boldsymbol{\phi}_h^{n-1}\right) \\
\mathbf{B} & \mathbf{0} & \mathbf{0} & \mathbf{0} \\
\hline
\mathbf{0} & \mathbf{0} & \mathbf{A}_s & -\mathbf{L}_s^\top \\
\hline
\mathbf{L}_f\left(\boldsymbol{\phi}_h^{n-1}\right) & \mathbf{0} & -\frac{1}{\Delta t}\mathbf{L}_s & \mathbf{0}
\end{array}\right)
\left(\begin{array}{c} \mathbf{u}^n \\ p^n \\ \hline \mathbf{d}^n \\ \hline \boldsymbol{\lambda}^n \end{array}\right)
=
\left(\begin{array}{c} \mathbf{f} \\ \mathbf{0} \\ \hline \mathbf{g} \\ \hline \mathbf{h} \end{array}\right)
\tag{11}
$$

and we employ a monolithic approach to solve this problem, ensuring both robustness and numerical stability.

Each block in global matrix (11) corresponds to a different physical contribution, Denoting with $\boldsymbol{\varphi}$, ψ, $\boldsymbol{\chi}$ and $\boldsymbol{\xi}$ the basis functions, of $\mathbf{V}_h$, Q_h, $\mathbf{W}_h$, $\boldsymbol{\Lambda}_h$, respectively, the matrices appearing in (11), have the following elements:

$$
\begin{aligned}
&\left(\mathbf{A}(\mathbf{u}_h^{n-1})\right)_{i,j} = \frac{\rho^f}{\Delta t}\left(\boldsymbol{\varphi}_i, \boldsymbol{\varphi}_j\right) + b(\mathbf{u}_h^{n-1}, \boldsymbol{\varphi}_j, \boldsymbol{\varphi}_i) + 2\mu\left(\boldsymbol{\epsilon}(\boldsymbol{\varphi}_i), \boldsymbol{\epsilon}(\boldsymbol{\varphi}_j)\right), \\
&(\mathbf{B})_{k,i} = -(\nabla \cdot \boldsymbol{\varphi}_i, \psi_k), \\
&(\mathbf{A}_s)_{i,j} = \frac{\rho^s \varepsilon}{\Delta t^2}\left(\boldsymbol{\chi}_i, \boldsymbol{\chi}_j\right)_\Sigma + \kappa(\nabla \boldsymbol{\chi}_j, \nabla \boldsymbol{\chi}_i)_\Sigma, \\
&\left(\mathbf{L}_f\left(\boldsymbol{\phi}_h^{n-1}\right)\right)_{\ell,j} = \left(\boldsymbol{\xi}_\ell, \boldsymbol{\varphi}_j\left(\boldsymbol{\phi}_h^{n-1}\right)_\Sigma\right), \quad (\mathbf{L}_s)_{\ell,j} = (\boldsymbol{\xi}_\ell, \boldsymbol{\chi}_j)_\Sigma.
\end{aligned}
$$

On the right-hand side, the forcing terms are given by:

$$
\mathbf{f}_i = \frac{\rho^f}{\Delta t}\left(\boldsymbol{\varphi}_i\, \mathbf{u}_h^{n-1}\right), \quad \mathbf{g}_i = \frac{\rho^s \epsilon}{\Delta t^2}\left(\boldsymbol{\chi}_i\, \left(2\mathbf{d}_h^{n-1} - \mathbf{d}_h^{n-2}\right)\right), \quad \mathbf{h}_\ell = -\frac{1}{\Delta t}\left(\boldsymbol{L}_s\, \boldsymbol{d}_h^{n-1}\right)_\ell.
$$

4 Numerical results

In the numerical tests, among the various possible engineering applications, we apply the method to the case of a venous blood vessel, following the benchmark data provided by [11]. These parameters include the physical characteristics of blood, the mechanical properties of the vessel wall, and the geometric dimensions of the vessel.

Blood is treated as an incompressible Newtonian fluid with a density $\rho_f = 1.0 \times 10^3$ kg/m^3 and a dynamic viscosity of $\mu = 35.0 \times 10^{-3}$ Pa $\cdot$ s.

The vessel wall is modeled as a thin, elastic structure with a Young's modulus of $E = 75.0 \times 10^3$ Pa and a Poisson's ratio of $\nu = 0.5$. The wall thickness is set to $\varepsilon = 1.0 \times 10^{-3}$ m, leading to an effective elastic coefficient $\kappa = 25.0$ Pa $\cdot$ m. The density of the vessel wall is $\rho_s = 1.1 \times 10^3$ kg/m^3, a typical value for biological soft tissues.

The vessel under consideration has a length of $L = 6.0 \times 10^{-2}$ m and a diameter of $H = 1.0 \times 10^{-2}$ m, which are representative dimensions for venous segments.

The numerical parameters include a time step of $\Delta t = 5.0 \times 10^{-3}$ s, ensuring adequate temporal resolution for capturing transient effects in the simulation.

We use two different velocity profiles at the inlet. The first one is constant in time and has the following parabolic profile:

$$u_{\text{in,s}}(x_2) = -\frac{4u_{\text{mean}}}{H^2}\, x_2^2 + \frac{4u_{\text{mean}}}{H}\, |x_2|,$$

where u_{mean} is the mean velocity of the fluid, set to 0.20 m/s. The second one models a pulsatile flow, and is defined as:

$$u_{\text{in,p}}(x_2, t) = u_{\text{in,s}}(x_2) + 0.4 \max\left(0, \sin\left(\frac{2\pi t}{T_{\text{pulse}}}\right)\right) u_{\text{in,s}}(x_2), \tag{12}$$

and T_{pulse} represents the characteristic period of the pulsatile flow, assumed equal to $T_{\text{pulse}} = 0.6$ s. In this way, it is possible to incorporate both a baseline steady flow and a pulsatile perturbation. A visualization of the pulsatile inflow is presented in Figure 2. This approach is designed to enforce a physiologically relevant inlet condition, capturing the temporal pulsation of the flow and the interaction with the elastic vessel, with enhanced realism.

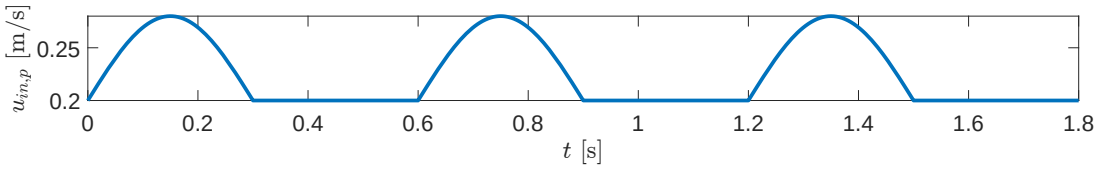

Figure 2: Inflow velocity profile at $\mathbf{x} = (0, -0.005)$.

Moreover, to solve the problem numerically, we consider a rectangular domain $\Omega = [0, L] \times [0, 2H]$, and we use a triangular mesh based on a structured grid with

36 subdivisions along the horizontal direction and 12 subdivisions along the vertical direction. The triangulation is constructed by first forming a regular grid of squares and then introducing diagonals within each square to obtain triangles.

Additionally, the midpoints of the vertical edges are connected by a horizontal segment $[0, L]$, representing the resting structure Σ. This horizontal segmentation consists of 35 subdivisions, forming an independent 1D mesh. As a result, the two meshes remain independent from each other (Figure 3).

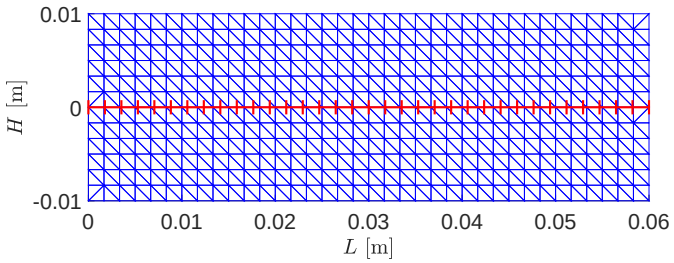

Figure 3: The two-dimensional mesh in Ω is displayed in blue, while in red is depicted the horizontal segment corresponds to Σ, with the intervals of its one-dimensional mesh.

All numerical test are conducted with `FreeFEM` [12] and the graphical outputs are generated using `ffmatlib` and `MATLAB` [13].

4.1 Comparison with remeshing strategy for fluid-structure interaction

A strongly coupled approach to fluid-structure interaction ensures consistency of the meshes between the fluid and structural domains. This method employs an iterative resolution, where fluid stresses drive solid deformation, altering the domain geometry and requiring continuous mesh updates. In turn, structural motion influences fluid behavior, necessitating kinematic coherence. The process alternates between solving the elastic problem on Σ and fluid equations in $\Omega^{\mathrm{f}}(t)$, remeshing iteratively until convergence is reached.

To assess the accuracy of the proposed fictitious method, we compare the results with those obtained using a classical numerical approach, based on a remeshing technique directly implementable in `FreeFEM`. For this comparison, we neglect the convection term in Equation (7), and we consider in Equation (5) $u_{\mathrm{in}} = u_{\mathrm{in,s}}(x_2)$. Starting from $\mathbf{u}_0 = (u_{\mathrm{mean}}, 0)$ in $\Omega^{\mathrm{f}}(t)$ and only for the fictitious method considering also $\mathbf{u}_0 = \mathbf{0}$ in $\Omega^{\mathrm{fd}}(t)$, the simulation runs for a time $t = 0.5$ s.

The comparison focuses on three key quantities: the fluid velocity, the fluid pressure, and the vertical displacement of the elastic structure. These quantities are evaluated at various representative points within the computational domains. Table 1

presents the numerical values obtained from both methods, and the results indicate that the proposed method provides a close approximation to the expected pressure distribution while maintaining comparable velocity accuracy. The structural displacement shows slight differences, although not physically relevant, which can be attributed to differences in numerical treatment at the fluid-structure interface.

Point	$\lvert\mathbf{u}\rvert$ (m/s)			p (Pa)			d_2 ($\times 10^{-4}$ m)		
	$\lvert\mathbf{u}\rvert_{\mathrm{F}}$	$\lvert\mathbf{u}\rvert_{\mathrm{R}}$	$\frac{\lvert\lvert\mathbf{u}\rvert_{\mathrm{R}}-\lvert\mathbf{u}\rvert_{\mathrm{F}}\rvert}{\lvert\mathbf{u}\rvert_{\mathrm{F}}}$	p_{F}	p_{R}	$\frac{\lvert p_{\mathrm{R}}-p_{\mathrm{F}}\rvert}{\lvert p_{\mathrm{F}}\rvert}$	$d_{2\mathrm{F}}$	$d_{2\mathrm{R}}$	$\frac{\lvert d_{2\mathrm{R}}-d_{2\mathrm{F}}\rvert}{\lvert d_{2F}\rvert}$
$(0.03, -0.005)$	0.1970	0.1969	0.0005	3.2252	3.2262	0.0003	–	–	–
$(0.04, -0.005)$	0.1960	0.1959	0.0005	2.1301	2.1524	0.01	–	–	–
$(0.05, -0.005)$	0.1953	0.1957	0.002	1.0456	1.0786	0.03	–	–	–
0.03	–	–	–	–	–	–	1.225	1.498	0.22
0.05	–	–	–	–	–	–	1.355	1.727	0.27

Table 1: Comparison of values and relative discrepancies of velocity, pressure, and displacement at selected spatial points between the fictitious method (F) and the classical method with remeshing (R) (the first points are located in the fluid and the coordinates are referred to Cartesian coordinates $\mathbf{x}$, while the last two points are located on Σ with Lagrangian coordinate L).

4.2 Simulation of a pulsatile flow

In this test we consider the fictitious domain method with fully unsteady Navier-Stokes equations for the fluid, and setting in Equation (5) $u_{\text{in}} = u_{\text{in,p}}(x_2, t)$.

As shown in Figure 4, spurious numerical oscillations occur near the outflow, indeed, to properly handle this type of artificial boundary and prevent unphysical reflection phenomena, we follow the approach proposed in [14]. A suitable terms is introduced to manage the pressure drop. Setting the data-driven value, estimated in relation to the shape and measure of the boundary $\Gamma^{\text{f}}_{\text{out}} \cup \Gamma^{\text{fd}}_{\text{out}}$, $V_{\text{ref}} = 0.9 \times 10^{-2}$ m/s as a reference velocity, we add an extra term to the matrix $\mathbf{A}$ in (11), i.e., $\mathbf{A} + \mathbf{V}^f_{\text{out}}$, and $\mathbf{V}^f_{\text{out}}$ has the following elements:

$$\left(\mathbf{V}^f_{\text{out}}\right)_{i,j} = \frac{1}{2}\,\rho^f\, V_{\text{ref}} \int_{\Gamma^{\text{f}}_{\text{out}} \cup \Gamma^{\text{fd}}_{\text{out}}} |\boldsymbol{\varphi}_j|\ (\boldsymbol{\varphi}_i \cdot \mathbf{n}^{\text{out}})\,.$$

In Figures 5, we display the fluid velocity and structural deformation progress during the evolution of the system, in response to inlet velocity variations. At $t = 0.15$ s, following the initial acceleration phase, the evolving flow field induces structural deformation. By $t = 0.30$ s, the inlet velocity reaches 0.20 m/s, leading to a slower flow and causing the structural deformation to shift downward from its rest position and until $t = 0.60$ s the system maintains this velocity values. At $t = 0.75$ s, a new acceleration phase intensifies fluid forces, further increasing flow velocity and structural deformation.

The evolution of the interface deformation is illustrated in Figure 6: the structural response over time is consistent with the periodic velocity profile in Equation (12) at inflow (as seen in Figure 2).

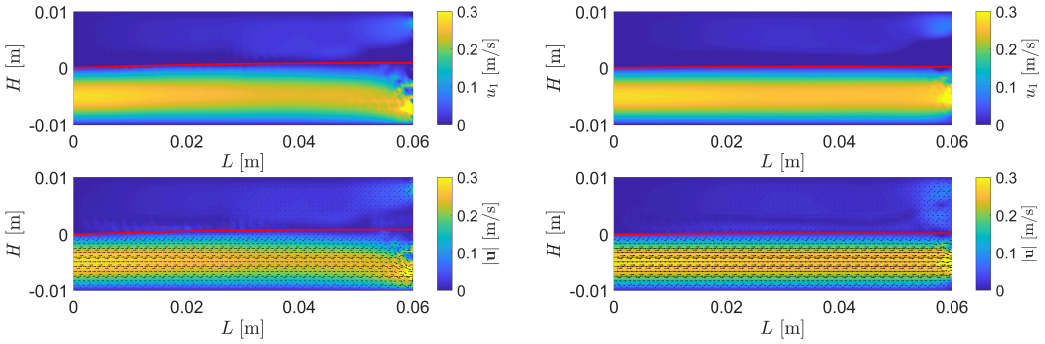

Figure 4: Velocity first component u_1, $|\mathbf{u}|$, velocity vectors and elastic structure position (depicted in red) at $t = 0.15$ s, with homogeneous Neumann boundary condition on $\Gamma^{\mathrm{f}}_{\mathrm{out}} \cup \Gamma^{\mathrm{fd}}_{\mathrm{out}}$ on the left, and with the additional term on outflow boundary on the right.

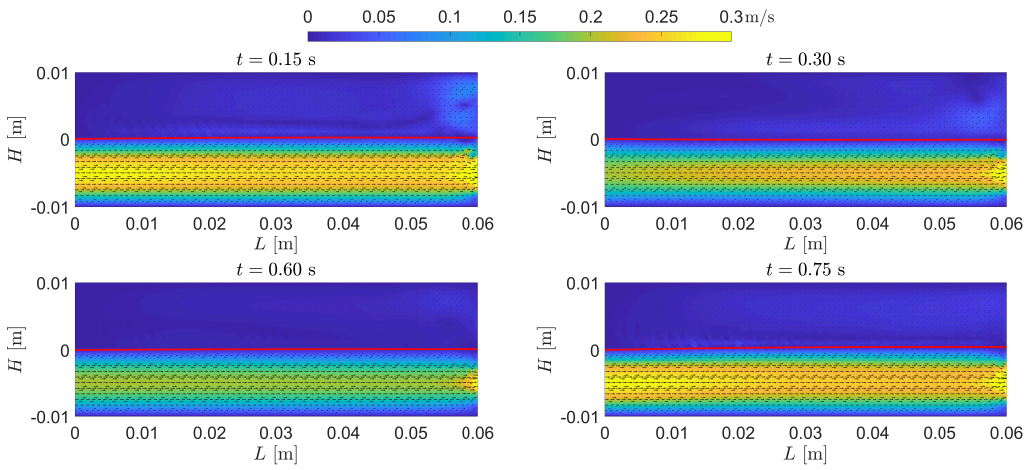

Figure 5: Velocity values $|\mathbf{u}|$, velocity vectors and elastic structure position (depicted in red) for various fixed times, for the test in Section 4.2.

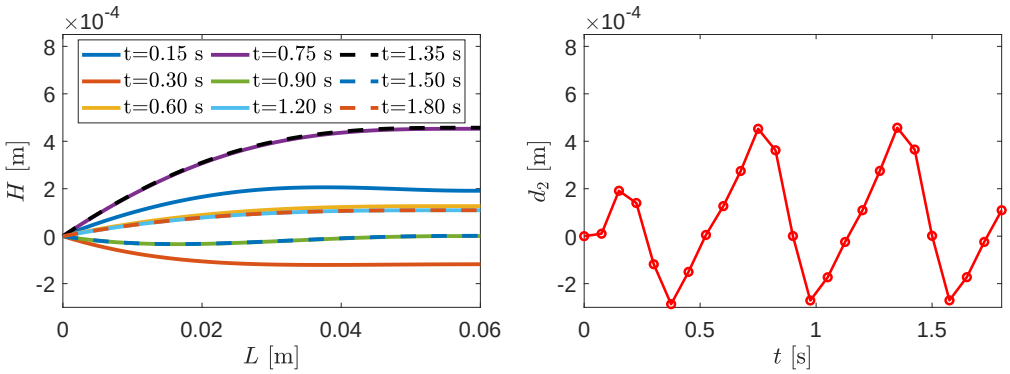

Figure 6: Superimposed interface profiles for various time steps on the left and the evolution of d_2 over time in $L = 0.06$ on the right.

5 Conclusions

We consider the flow of a Newtonian fluid in a channel with deformable walls. The deformation of the solid wall is governed by a linear elasticity model. In order to avoid the need of adapting the mesh in the moving fluid region, we use a fictitious domain approach. This consists in extending the Navier-Stokes equations in a fixed domain containing both the fluid and the solid domains, and recovering the physical solution by the addition of a Lagrange multiplier associated with the continuity constraint for the velocities. In order to prevent spurious effects in the physical domain, we introduce a modification of the Neumann conditions at the outflow boundary.

The proposed method is applied to the case of blood flow in a venous vessel, using physiologically relevant parameters. The simulations enables the capture of both the fluid velocity evolution and the deformation dynamics of the elastic wall, providing a comprehensive description of the fluid–structure interaction. The comparison of this approach with a classical remeshing-based method presents a satisfactory agreement, supporting the validity of the proposed formulation.

It turns out that the fictitious domain approach may simplify the numerical discretization, since it avoids the construction of a fluid mesh fitted with the deformation of the solid which can be computationally expensive. On the other hand this approach requires to compute the so-called coupling matrix which takes into account the relation between the fluid and the solid mesh.

Acknowledgements

The authors are member of INdAM Research group GNCS. The research of L. Gastaldi is is partially supported by PRIN/MUR (grant No.20227K44ME) and IMATI/CNR.

References

[1] T. Belytschko, “Fluid-structure interaction”, Computers & Structures, 12(4), 459-469, 1980.

[2] P. Le Tallec, J. Mouro, “Fluid structure interaction with large structural displacements”, Computer Methods in Applied Mechanics and Engineering 190(24–25,) 3039-3067, 2001.

[3] A. Quarteroni, L. Formaggia, “Mathematical Modelling and Numerical Simulation of the Cardiovascular System”, Handbook of Numerical Analysis, 12, 3-127, 2004.

[4] G. Hou, J. Wang, A. Layton, “Numerical Methods for Fluid-Structure Interaction — A Review”, Communications in Computational Physics, 12, 337–77, 2012.

[5] C.S. Peskin, “Flow patterns around heart valves: A numerical method”, Journal of Computational Physics, 10(2), 252-271, 1972.

[6] D. Boffi, N. Cavallini, L. Gastaldi, “The Finite Element Immersed Boundary Method with Distributed Lagrange Multiplier”, SIAM Journal on Numerical Analysis, 53(6), 2584–2604, 2015.

[7] M. Annese , M.A. Fernández, L. Gastaldi, “Splitting Schemes for a Lagrange Multiplier Formulation of FSI with Immersed Thin-Walled Structure: Stability and Convergence Analysis”, IMA Journal of Numerical Analysis, 43(2), 881–919, 2023.

[8] R. Glowinski, T.-W. Pan, and J. Periaux, ”A Lagrange multiplier/fictitious domain method for the numerical simulation of incompressible viscous flow around moving rigid bodies:(i) case where the rigid body motions are known a priori”, Comptes Rendus de l’Académie des Sciences-Series I-Mathematics, 324(3), 361-369, 1997.

[9] R. Glowinski, T.-W. Pan, T. I. Hesla, D. D. Joseph, and J. Periaux, ”A fictitious domain approach to the direct numerical simulation of incompressible viscous flow past moving rigid bodies: application to particulate flow”, Journal of Computational Physics, 169(2), 363-426, 2001.

[10] D. Boffi, F. Brezzi, M. Fortin, “Mixed Finite Element Methods and Applications”, Springer eBooks. Berlin, Springer, 2013.

[11] L. Formaggia, J.F. Gerbeau, F. Nobile, A. Quarteroni, “On the Coupling of 3D and 1D Navier-Stokes Equations for Flow Problems in Compliant Vessels”, Computer Methods in Applied Mechanics and Engineering 191(6), 561–582, 2001.

[12] F. Hecht, “New development in FreeFem++”, Journal of Numerical Mathematics, 20(3-4), 251-266, 2012.

[13] MATLAB version: 24.1.0 (R2024a), Natick, Massachusetts: The MathWorks Inc., 2024.

[14] J.G. Heywood, R. Rannacher, S. Turek, “Artificial Boundaries and Flux and Pressure Conditions for the Incompressible Navier-Stokes Equations”, International Journal for Numerical Methods in Fluids 22(5), 325–52, 1996.